PHOTONICS Research

Visible Kerr comb generation in a high-Q silica microdisk resonator with a large wedge angle

Jiyang Ma,[1,†] Longfu Xiao,[1,†] Jiaxin Gu,[1,†] Hao Li,[1] Xinyu Cheng,[1] Guangqiang He,[2] Xiaoshun Jiang,[1,*] and Min Xiao[1,3]

[1]National Laboratory of Solid State Microstructures, College of Engineering and Applied Sciences and School of Physics, Nanjing University, Nanjing 210093, China
[2]State Key Laboratory of Advanced Optical Communication Systems and Networks, Department of Electronic Engineering, Shanghai Jiao Tong University, Shanghai 200240, China
[3]Department of Physics, University of Arkansas, Fayetteville, Arkansas 72701, USA
*Corresponding author: jxs@nju.edu.cn

Received 4 January 2019; revised 14 March 2019; accepted 14 March 2019; posted 14 March 2019 (Doc. ID 356704); published 25 April 2019

This paper describes the specially designed geometry of a dry-etched large-wedge-angle silica microdisk resonator that enables anomalous dispersion in the 780 nm wavelength regime. This anomalous dispersion occurs naturally without the use of a mode-hybridization technique to control the geometrical dispersion. By fabricating a 1-μm-thick silica microdisk with a wedge angle as large as 56° and an optical Q-factor larger than 10^7, we achieve a visible Kerr comb that covers the wavelength interval of 700–897 nm. The wide optical frequency range and the closeness to the clock transition at 698 nm of ^{87}Sr atoms make our visible comb a potentially useful tool in optical atomic clock applications. © 2019 Chinese Laser Press

https://doi.org/10.1364/PRJ.7.000573

1. INTRODUCTION

Optical frequency combs are coherent light sources with a large number of evenly spaced frequency lines, which can be exploited in many scientific applications [1–4]. Compared with traditional optical frequency combs based on large-size mode-locked lasers that cannot be integrated on chip [1], the up-to-date Kerr-type microcombs [5,6] based on cascaded four-wave-mixing processes possess many significant advantages. These include a compact size, low optical loss, and feasibility of on-chip integration [5–8]. Since their invention, this field has garnered tremendous attention and enjoyed rapid progress. Kerr-type microcombs have been realized in many platforms [9–22], some of which are already integrated on chip. After successfully generating optical frequency combs in different material systems, many studies have been geared up toward potential applications, such as arbitrary waveform generation [19], coherent optical communication [23], optical synthesizer [24], ultrafast optical ranging [25,26], and astronomical spectrum calibration [27,28]. So far, most of the Kerr frequency microcombs and their corresponding applications have been realized in the wavelength near 1550 nm [9–22]. The generation of the visible microcombs that are desirable for optical atomic clocks and optical coherence tomography is still challenging due to the strong normal dispersion induced by the material and the lower optical quality factor of the microcavity in the visible wavelength region.

Recently, several approaches have been employed to generate visible Kerr combs [29–38], such as using second-harmonic/third-harmonic generation [29–33] to translate a near-infrared comb to the visible range or designing a peculiar geometry possessing large anomalous dispersion to overcome the inherent normal dispersion of the material [34–38]. However, all those methods suffer from certain disadvantages, such as a narrow visible bandwidth [34,35], large pump power needed [31,33,37,38], limited conversion efficiency [29–32], non-integrated platforms [34,35], limited visible comb line power [37], and rigidities in fabrication [36].

In this work, we present a new method of visible comb generation. By employing a large-wedge-angle silica microdisk resonator with a thickness of 1 μm, the normal dispersion of silica material in the 780 nm regime can be completely compensated by its geometric dispersion. As a result, we obtain a resonator that produces anomalous dispersion in the visible wavelength regime without using mode hybridization, so that a visible comb can be generated directly without using any frequency conversion technique. As is shown in the next section, the microdisk possesses anomalous dispersion over the thicknesses of 800–1200 nm, which makes the fabrication process less stringent than the method by Lee *et al.* [36]. Furthermore, the visible comb obtained in our experiment covers the wavelengths ranging from 700 nm to 897 nm. To the best of our

knowledge, this is the broadest wavelength range among the experimentally demonstrated visible Kerr combs.

2. DEVICE FABRICATION AND DISPERSION SIMULATION

The experiment conducted in this study uses the silica microdisk resonator shown in Fig. 1. The fabrication process is similar to that described in our previous work [39,40]. The disk is 1 μm thick with a diameter of 80 μm. The most intriguing feature of our disk is the large wedge angle of 56° (the definition of the wedge angle is illustrated in Fig. 2(a), and it is indicated by angle α), which is usually hard to attain if the silica microdisk is fabricated by wet etching [41]. It is this special geometry that allows our disk to overcome the large normal dispersion induced by the silica material and naturally exhibit anomalous dispersion in the 780 nm wavelength regime. In previous studies where buffered hydrofluoric acid (HF) was used to etch a thicker silica disk (~1.5 μm thickness), the wedge angle could not reach this level, and mode hybridization was employed to enable the small-wedge-angle disks to provide anomalous dispersion at ~780 nm [36]. However, this produced extra problems in the fabrication process, namely that the disk's thickness should not deviate by more than 50 nm, as mode hybridization is very sensitive to the thickness of the disk. On the contrary, our disk displays the feature of a large wedge angle, and it naturally exhibits anomalous dispersion in the 780 nm wavelength region, independent of mode hybridization [see Figs. 2(c) and 2(d)].

Before conducting the experiment, we first simulate the dispersion characteristics of our disk using the standard finite-element method (FEM) [42]. Figure 2(a) schematically illustrates the mode profile of the fundamental TM10 mode (we define the first mode number according to the maximum intensity in the radial direction, while the second mode number is defined as $l - m$ for m and l as defined in Ref. [43]), which we harness as the pump mode in the subsequent experiment inside our cavity. Figure 2(b) shows the dispersion relationship with respect to the wavelength of the cavity used in the experiment. As one can see, the TM10 mode shows the anomalous dispersion characteristics ($D > 0$) at 780 nm. Figure 2(c) presents the dispersion characteristics of the TM10 mode at the 780 nm wavelength for different disk thicknesses and different wedge angles. It is clear that a wedge angle of 56° provides an anomalous dispersion over a large thickness range between 0.8 and 1.2 μm; additionally, the anomalous dispersion is insensitive to the wedge angle. These characteristics greatly reduce the constraints put on the disk thickness and the wedge angle, thus making fabrication significantly easier than the method by Lee *et al.* [36], in which the disk thickness has a tolerance of only 50 nm. Figure 2(d) depicts the effective index at different thicknesses for different mode families at a wedge angle of 56° and a wavelength of 780 nm. The smooth and continuous variation behaviors of the dispersion and effective refractive index with the disk's thickness in Figs. 2(c) and 2(d) indicate that our disk does not exhibit the characteristics of mode hybridization [36].

Figure 2(e) shows the variation of zero dispersion wavelengths with different wedge angles for the silica microdisk resonators that are 1 μm in thickness and with a 80 μm diameter. It is clear that when increasing the wedge angle, the zero dispersion wavelength will shift to a shorter wavelength [39]. Figure 2(f) illustrates the dispersion character of the TM10 mode for a 56° wedge angle silica disk with a diameter of 2 mm. The zero dispersion wavelength can be shifted to ~680 nm, which is beneficial for visible comb generation with a shorter wavelength, as well as a lower repetition rate.

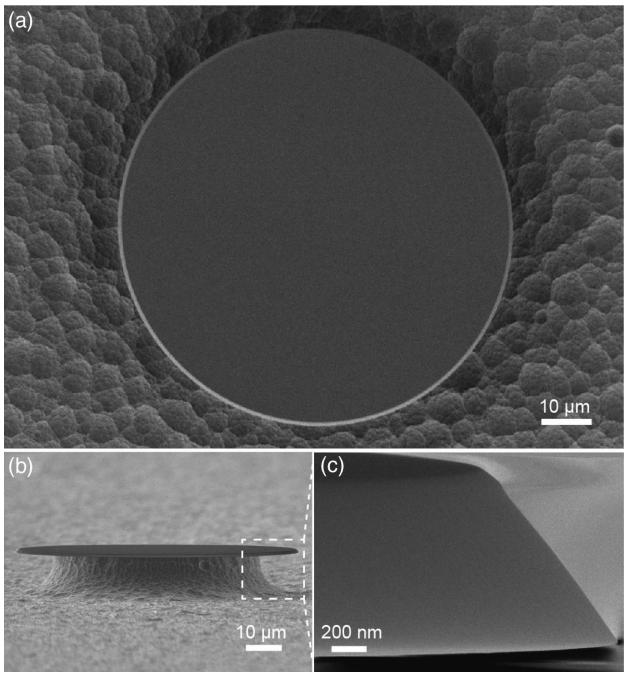

Fig. 1. SEM images of the large-wedge-angle microdisk resonator used in our experiment. (a), (b) Full-scale view of the microresonator. (c) Close-up of the microresonator to show the detailed characteristics of the large wedge angle.

3. *Q*-FACTOR AND THRESHOLD MEASUREMENT

We now describe an experiment using the setup shown in Fig. 3(c). First, we test the quality factor (Q) of our cavity by sending a scanning laser into the cavity and measuring the linewidth of the transmitted Lorentz peak, as illustrated in Fig. 3(a). The doublet resonance dip is due to the coupling between the clockwise and counter-clockwise traveling modes induced by surface roughness [44]. The microdisk resonator has the intrinsic and loaded Q factors of 1.08×10^7 and 0.98×10^7, respectively.

Next, we measure the threshold power of the optical parametric oscillation (OPO). We find the OPO process occurs at the threshold power of 1.62 mW (launched power in fiber). The formula of the OPO threshold power can be written as [14,45]

$$P_{\mathrm{th}} = \frac{V_0 n_0^2 \omega}{8 n_2 c \eta Q^2},$$

where V_0 is the effective mode volume, n_0 is the refractive index of silica, $\omega/2\pi$ denotes the resonance frequency, n_2 represents the nonlinear refractive index of silica, c is the speed of

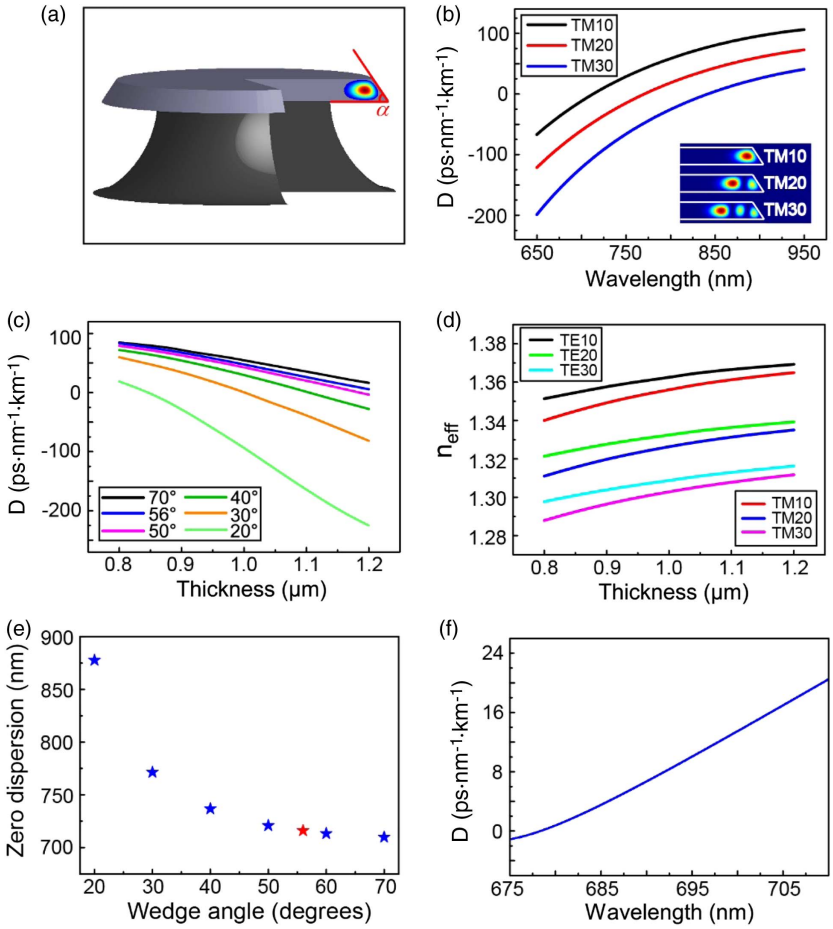

Fig. 2. (a) Illustration of the mode profile for the fundamental TM10 mode inside the cavity. An indication of angle α shows the definition of the wedge angle. (b) Dispersion characteristics of the TM10, TM20, TM30 modes for the disk 80 μm in diameter, 1 μm in thickness, and a 56° wedge angle. Inset: simulated mode profiles of the TM10, TM20 and TM30 modes, respectively. (c) Variation of the dispersion at the wavelength 780 nm when changing the thickness of the disk at different wedge angles. The diameter is kept at 80 μm, and the used cavity mode for the simulation is the TM10 mode. (d) Variation of the effective index by changing the thickness of the disk for different mode families at the wavelength of 780 nm; during the simulation, the wedge angle and diameter are fixed at 56° and 80 μm, respectively. (e) Variation of the zero dispersion wavelength for the TM10 mode with different wedge angles. The diameter of the microdisk cavity is 80 μm, and the thickness of the microcavity is 1 μm. The red star indicates the angle of the silica microdisk resonator used in the experiment. (f) Dispersion of the TM10 mode for a 56° wedge angle silica disk, 1 μm in thickness and 2 mm in diameter.

light in vacuum, η is the coupling rate, and Q denotes the loaded Q-factor of the cavity. The measured threshold power matches quite well with the theoretical value. The deviation of linear behavior of the last data point in threshold measurement is due to the energy transfer of the first sideband to the second sideband.

4. VISIBLE KERR-COMB GENERATION

Finally, we pump the disk above its OPO threshold power and gradually increase the pump power, while observing the evolution of the optical spectrum of the generated visible comb without using any extra frequency conversion technique. Figure 4 shows the optical spectra produced by pumping the cavity with launched optical powers of 21.50 mW, 28.50 mW, and 36.50 mW, respectively. The pump wavelength is fixed at 780 nm, where the disk possesses an anomalous dispersion. During the whole experiment the microdisk resonator is over-coupled to the tapered fiber in order to maintain a mechanical stability. As shown in Fig. 4(a), only the primary combs dominate in the spectrum when the pumping power is at a relatively low level [46]. By controlling parameters like the frequency detuning of the pump laser or the coupling rate between the fiber taper and the optical microcavity, the position of the primary comb can be altered [46]. By further increasing the pump power after the emergence of the primary combs, sub-combs will be generated [46], filling the gaps between primary comb lines, as is illustrated in Figs. 4(b) and 4(c). In Fig. 4(c), the visible comb contains as many as 112 optical frequency lines covering the optical wavelengths from 700 nm to 897 nm. We should stress that 700 nm is the shortest wavelength achieved in any experimentally demonstrated visible Kerr combs that do not use a frequency conversion technique, and the wavelength range of our visible comb is also broader than any one reported in previous studies [29–38]. Importantly,

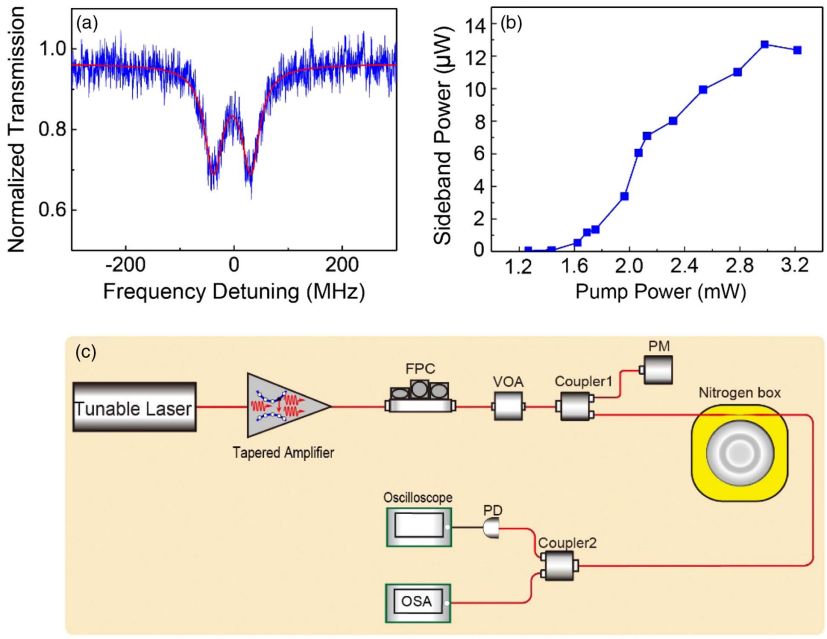

Fig. 3. (a) Measured transmission spectrum of the disk used to generate the visible comb; the corresponding intrinsic and loaded Q-factors are 1.08×10^7 and 0.98×10^7, respectively. (b) Variation of the side band power with the pump power; the OPO threshold is 1.62 mW. (c) Experimental setup: FPC, fiber polarization controller; PM, power meter; VOA, variable optical attenuator; OSA, optical spectrum analyzer; PD, photo diode.

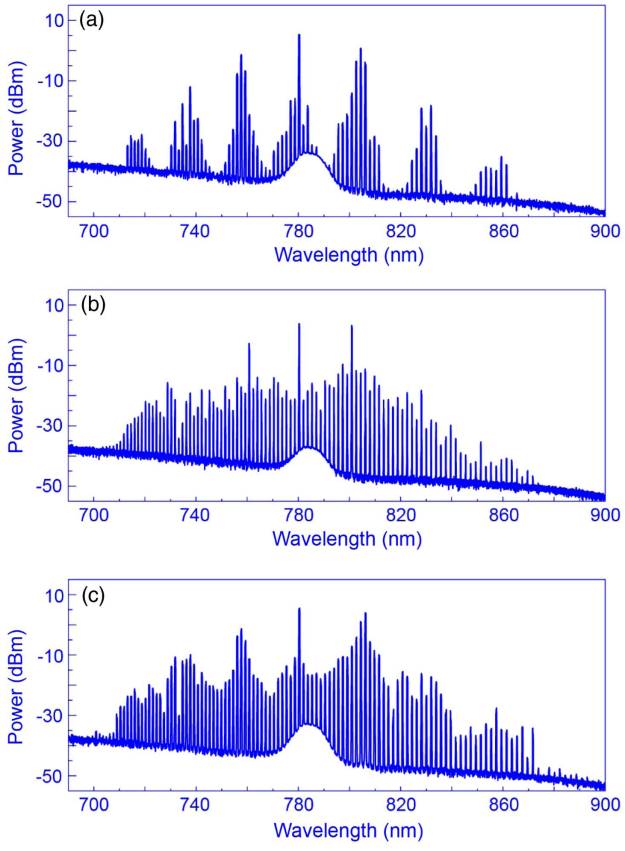

Fig. 4. Generation of visible Kerr combs with different pump powers. (a) Visible Kerr comb generated with a launched pump power of 21.50 mW. (b) Visible Kerr comb generated with a launched pump power of 28.50 mW. (c) Visible Kerr comb generated with a launched pump power of 36.50 mW.

the comb line at the shortest wavelength is very close to the $^1S_0 - {}^3P_0$ transition at 698 nm of ^{87}Sr atoms [2], and it has potential to be further exploited in precise and accurate, as well as compact, optical clocks.

5. SUMMARY

We have successfully generated a visible Kerr microcomb using our specially designed large-wedge-angle silica microdisk. The geometry of the microdisk enables the appearance of anomalous dispersion to occur naturally in the 780 nm wavelength range without the use of mode hybridization. We can directly produce efficient visible Kerr combs by pumping the cavity at 780 nm without requiring any frequency conversion technique. The larger tolerances in the disk's thickness and wedge angle greatly reduce the difficulties in the device fabrication, making it more versatile for practical applications. Additionally, our visible microcomb covers the wavelength range from 700 nm to 897 nm, which, to the best of our knowledge, is the broadest optical wavelength range of any experimentally demonstrated visible Kerr combs. Such chip-based visible microcombs will find applications in optical coherence tomography and strontium optical lattice clocks. In the future, we will attempt to pump our microcavity at a shorter wavelength so that the comb lines can be extended to the wavelengths below 698 nm to reach the ^{87}Sr clock transition. Also, the disk wedge angle and other geometrical parameters can be further explored to shift the zero dispersion point to a shorter wavelength and expand the wavelengths of the microcomb in the visible and ultraviolet ranges. By optimizing the fabrication process of the microdisk cavity with a larger diameter, we expect to achieve a visible Kerr-comb to a shorter wavelength with a

detectable repetition rate and access it in a stable soliton state [47] using the dry-etched silica microcavity.

Funding. National Key R&D Program of China (2016YFA0302500, 2017YFA0303703); National Natural Science Foundation of China (NSFC) (61435007, 11574144, 11621091, 61475099).

Acknowledgment. The authors thank Dr. Hong Chang for helpful discussions. We also thank Han Wang and Dr. Xuewei Wu for technical assistance.

†These authors contributed equally to this work.

REFERENCES

1. T. Udem, R. Holzwarth, and T. W. Hänsch, "Optical frequency metrology," Nature **416**, 233–237 (2002).
2. A. D. Ludlow, M. M. Boyd, and J. Ye, "Optical atomic clocks," Rev. Mod. Phys. **87**, 637–701 (2015).
3. R. Holzwarth, T. Udem, T. W. Hänsch, J. C. Knight, W. J. Wadsworth, and P. St. J. Russell, "Optical frequency synthesizer for precision spectroscopy," Phys. Rev. Lett. **85**, 2264–2267 (2000).
4. T. Steinmetz, T. Wilken, C. Araujo-Hauck, R. Holzwarth, T. W. Hänsch, L. Pasquini, A. Manescau, S. D'Odorico, M. T. Murphy, T. Kentischer, W. Schmidt, and T. Udem, "Laser frequency combs for astronomical observations," Science **321**, 1335–1337 (2008).
5. T. J. Kippenberg, R. Holzwarth, and S. A. Diddams, "Microresonator-based optical frequency combs," Science **332**, 555–559 (2011).
6. P. Del'Haye, A. Schliesser, O. Arcizet, T. Wilken, R. Holzwarth, and T. J. Kippenberg, "Optical frequency comb generation from a monolithic microresonator," Nature **450**, 1214–1217 (2007).
7. Y. Li, X. Jiang, G. Zhao, and L. Yang, "Whispering gallery mode microresonator for nonlinear photonics," arXiv: 1809.04878 (2017).
8. G. Lin, A. Coillet, and Y. K. Chembo, "Nonlinear photonics with high-*Q* whispering-gallery-mode resonators," Adv. Opt. Photon. **9**, 828–890 (2017).
9. A. A. Savchenkov, A. B. Matsko, V. S. Ilchenko, I. Solomatine, D. Seidel, and L. Maleki, "Tunable optical frequency comb with a crystalline whispering gallery mode resonator," Phys. Rev. Lett. **101**, 093902 (2008).
10. I. S. Grudinin, N. Yu, and L. Maleki, "Generation of optical frequency combs with a CaF_2 resonator," Opt. Lett. **34**, 878–880 (2009).
11. S. B. Papp and S. A. Diddams, "Spectral and temporal characterization of a fused-quartz-microresonator optical frequency comb," Phys. Rev. A **84**, 053833 (2011).
12. B. J. M. Hausmann, I. Bulu, V. Venkataraman, P. Deotare, and M. Lonar, "Diamond nonlinear photonics," Nat. Photonics **8**, 369–374 (2014).
13. H. Jung, C. Xiong, K. Y. Fong, X. Zhang, and H. X. Tang, "Optical frequency comb generation from aluminum nitride microring resonator," Opt. Lett. **38**, 2810–2813 (2013).
14. T. Herr, K. Hartinger, J. Riemensberger, C. Y. Wang, E. Gavartin, R. Holzwarth, M. L. Gorodetsky, and T. J. Kippenberg, "Universal formation dynamics and noise of Kerr-frequency combs in microresonators," Nat. Photonics **6**, 480–487 (2012).
15. M. A. Foster, J. S. Levy, O. Kuzucu, K. Saha, M. Lipson, and A. L. Gaeta, "Silicon-based monolithic optical frequency comb source," Opt. Express **19**, 14233–14239 (2011).
16. Q. Lu, S. Liu, X. Wu, L. Liu, and L. Xu, "Stimulated Brillouin laser and frequency comb generation in high-*Q* microbubble resonators," Opt. Lett. **41**, 1736–1739 (2016).
17. J. S. Levy, A. Gondarenko, M. A. Foster, A. C. Turner-Foster, A. L. Gaeta, and M. Lipson, "CMOS-compatible multiple-wavelength oscillator for on-chip optical interconnects," Nat. Photonics **4**, 37–40 (2010).
18. L. Razzari, D. Duchesne, M. Ferrera, R. Morandotti, S. Chu, B. E. Little, and D. J. Moss, "CMOS-compatible integrated optical hyperparametric oscillator," Nat. Photonics **4**, 41–45 (2010).
19. F. Ferdous, H. Miao, D. E. Leaird, K. Srinivasan, J. Wang, L. Chen, L. T. Vargheses, and A. M. Weiner, "Spectral line-by-line pulse shaping of on-chip microresonator frequency combs," Nat. Photonics **5**, 770–776 (2011).
20. J. Li, H. Lee, T. Chen, and K. J. Vahala, "Low-pump-power, low phase-noise, and microwave to millimeter-wave repetition rate operation in microcombs," Phys. Rev. Lett. **109**, 233901 (2012).
21. J. Ma, X. Jiang, and M. Xiao, "Kerr frequency combs in large-size, ultra-high-*Q* toroid microcavities with low repetition rates," Photon. Res. **5**, B54–B58 (2017).
22. T. Herr, V. Brasch, J. D. Jost, C. Y. Wang, N. M. Kondratiev, M. L. Gorodetsky, and T. J. Kippenberg, "Temporal solitons in optical microresonators," Nat. Photonics **8**, 145–152 (2014).
23. P. M. Palomo, J. N. Kemal, M. Karpov, A. Kordts, J. Pfeifle, M. H. P. Pfeiffer, P. Trocha, S. Wolf, V. Brasch, M. H. Anderson, R. Rosenberger, K. Vijayan, W. Freude, T. J. Kippenberg, and C. Koos, "Microresonator-based solitons for massively parallel coherent optical communications," Nature **546**, 274–279 (2017).
24. D. T. Spencer, T. Drake, T. C. Briles, J. Stone, L. C. Sinclair, C. Fredrick, Q. Li, D. Westly, B. R. Ilic, A. Bluestone, N. Volet, T. Komljenovic, L. Chang, S. H. Lee, D. Y. Oh, M.-G. Suh, K. Y. Yang, M. H. P. Pfeiffer, T. J. Kippenberg, E. Norberg, L. Theogarajan, K. Vahala, N. R. Newbury, K. Srinivasan, J. E. Bowers, S. A. Diddams, and S. B. Papp, "An optical-frequency synthesizer using integrated photonics," Nature **557**, 81–85 (2018).
25. M.-G. Suh and K. J. Vahala, "Soliton microcomb range measurement," Science **359**, 884–887 (2018).
26. P. Trocha, M. Karpov, D. Ganin, M. H. P. Pfeiffer, A. Kordts, S. Wolf, J. Krockenberger, P. Marin-Palomo, C. Weimann, S. Randel, W. Freude, T. J. Kippenberg, and C. Koos, "Ultrafast optical ranging using microresonator soliton frequency combs," Science **359**, 887–891 (2018).
27. E. Obrzud, M. Rainer, A. Harutyunyan, M. H. Anderson, J. Liu, M. Geiselmann, B. Chazelas, S. Kundermann, S. Lecomte, M. Cecconi, A. Ghedina, E. Molinari, F. Pepe, F. Wildi, F. Bouchy, T. J. Kippenberg, and T. Herr, "A microphotonic astrocomb," Nat. Photonics **13**, 31–35 (2019).
28. M.-G. Suh, X. Yi, Y.-H. Lai, S. Leifer, I. S. Grudinin, G. Vasisht, E. C. Martin, M. P. Fitzgerald, G. Doppmann, J. Wang, D. Mawet, S. B. Papp, S. A. Diddams, C. Beichman, and K. Vahala, "Searching for exoplanets using a microresonator astrocomb," Nat. Photonics **13**, 25–30 (2019).
29. X. Xue, F. Leo, Y. Xuan, J. A. Jaramillo-Villegas, P.-H. Wang, D. E. Leaird, M. Erkintalo, M. Qi, and A. M. Weiner, "Second-harmonic-assisted four-wave mixing in chip-based microresonator frequency comb generation," Light Sci. Appl. **6**, e16253 (2017).
30. H. Jung, R. Stoll, X. Guo, D. Fischer, and H. X. Tang, "Green, red, and IR frequency comb line generation from single IR pump in AlN microring resonator," Optica **1**, 396–399 (2014).
31. L. Wang, L. Chang, N. Volet, M. H. P. Pfeiffer, M. Zervas, H. Guo, T. J. Kippenberg, and J. E. Bowers, "Frequency comb generation in the green using silicon nitride microresonators," Laser Photon. Rev. **10**, 631–638 (2016).
32. X. Liu, C. Sun, B. Xiong, L. Wang, Y. Han, Z. Hao, H. Li, Y. Luo, J. Yan, T. Wei, Y. Zhang, and J. Wang, "Generation of multiple near-visible comb lines in an AlN microring via $\chi^{(2)}$ and $\chi^{(3)}$ optical nonlinearities," Appl. Phys. Lett. **113**, 171106 (2018).
33. X. Guo, C.-L. Zou, H. Jung, Z. Gong, A. Bruch, L. Jiang, and H. X. Tang, "Efficient generation of a near-visible frequency comb via Cherenkov-like radiation from a Kerr microcomb," Phys. Rev. Appl. **10**, 014012 (2018).
34. A. A. Savchenkov, A. B. Matsko, W. Liang, V. S. Ilchenko, D. Seidel, and L. Maleki, "Kerr combs with selectable central frequency," Nat. Photonics **5**, 293–296 (2011).
35. Y. Yang, X. Jiang, S. Kasumie, G. Zhao, L. Xu, J. M. Ward, L. Yang, and S. N. Chormaic, "Four-wave mixing parametric oscillation and frequency comb generation at visible wavelengths in a silica microbubble resonator," Opt. Lett. **41**, 5266–5269 (2016).

36. S. H. Lee, D. Y. Oh, Q.-F. Yang, B. Shen, H. Wang, K. Y. Yang, Y. H. Lai, X. Yi, and K. Vahala, "Towards visible soliton microcomb generation," Nat. Commun. **8**, 1295 (2017).
37. M. Karpov, M. H. P. Pfeiffer, J. Liu, A. Lukashchuk, and T. J. Kippenberg, "Photonic chip-based soliton frequency combs covering the biological imaging window," Nat. Commun. **9**, 1146 (2018).
38. P. S. Donvalkar, F. A. S. Barbosa, X. Ji, Y. Okawachi, R. Mcnally, A. Farsi, A. Klenner, M. Lipson, and A. L. Gaeta, "Broadband frequency comb generation in the near-visible using higher-order modes in silicon nitride microresonators," in *Conference on Lasers and Electro-Optics* (2017), paper STu4J.5.
39. G. Li, P. Liu, X. Jiang, C. Yang, J. Ma, H. Wu, and M. Xiao, "High-*Q* silica microdisk optical resonators with large wedge angles on a silicon chip," Photon. Res. **3**, 279–282 (2015).
40. X. Jiang, Q. Lin, J. Rosenberg, K. Vahala, and O. Painter, "High-*Q* double-disk microcavities for cavity optomechanics," Opt. Express **17**, 20911–20919 (2009).
41. H. Lee, T. Chen, J. Li, K. Y. Yang, S. Jeon, O. Painter, and K. J. Vahala, "Chemically etched ultrahigh-*Q* wedge-resonator on a silicon chip," Nat. Photonics **6**, 369–373 (2012).
42. M. Oxborrow, "Traceable 2D finite-element simulation of the whispering gallery modes of axisymmetric electromagnetic resonators," IEEE Trans. Microwave Theory Tech. **55**, 1209–1218 (2007).
43. M. L. Gorodetsky and V. S. Ilchenko, "High-*Q* optical whispering-gallery microresonators: precession approach for spherical mode analysis and emission patterns with prism couplers," Opt. Commun. **113**, 133–143 (1994).
44. T. J. Kippenberg, S. M. Spillane, and K. J. Vahala, "Modal coupling in traveling-wave resonators," Opt. Lett. **27**, 1669–1671 (2002).
45. T. J. Kippenberg, S. M. Spillane, and K. J. Vahala, "Kerr-nonlinearity optical parametric oscillation in an ultrahigh-*Q* toroid microcavity," Phys. Rev. Lett. **93**, 083904 (2004).
46. Y. K. Chembo and N. Yu, "Modal expansion approach to optical-frequency-comb generation with monolithic whispering-gallery-mode resonators," Phys. Rev. A **82**, 033801 (2010).
47. T. J. Kippenberg, A. L. Gaeta, M. Lipson, and M. L. Gorodetsky, "Dissipative Kerr solitons in optical microresonators," Science **361**, eaan8083 (2018).